J. Synchrotron Rad. (2000). **7**, 405–410

Transmission phase gratings for EUV interferometry

Patrick P. Naulleau,[a]* Chang Hyun Cho,[b] Eric M. Gullikson[a] and Jeffrey Bokor[a,b]

[a]Center for X-ray Optics, Lawrence Berkeley National Laboratory, Berkeley, CA 94720, USA, and [b]EECS Department, University of California, Berkeley, CA 94720, USA. E-mail: pnaulleau@lbl.gov

(*Received 24 April 2000; accepted 28 July 2000*)

The performance of the recently developed EUV phase-shifting point diffraction interferometer (PS/PDI) depends heavily on the characteristics of the grating beamsplitter used in the implementation. Ideally, such a grating should provide throughput of better than 25% and diffraction efficiency, defined as the ratio of the first-diffracted-order power to the zero-order power, variable in the range from approximately 10 to 500. The optimal method for achieving these goals is by way of a phase grating. Also, PS/PDI system implementation issues favor the use of transmission gratings over reflection gratings. Here, the design, fabrication, and characterization of a recently developed transmission phase grating developed for use in EUV interferometry is described.

Keywords: EUV; phase gratings; diffraction; interferometry.

1. Introduction

The recent development of extreme ultraviolet (EUV) optics for use in next-generation projection lithography systems has led to several advancements in EUV interferometry (Bjorkholm *et al.*, 1995; Ray-Chaudhuri *et al.*, 1995; Medecki *et al.*, 1996). With a demonstrated reference-wavefront accuracy of better than $\lambda_{EUV}/350$ (0.04 nm at λ_{EUV} = 13.4 nm) (Naulleau *et al.*, 1999), the phase-shifting point diffraction interferometer (PS/PDI) (Medecki *et al.*, 1996; Goldberg, 1997; Tejnil *et al.*, 1997) is, to the best of our knowledge, the highest-accuracy EUV interferometer available. In practice, however, it may not be possible to achieve this accuracy due to limitations imparted by the grating used as the beamsplitting device. Here we describe the fabrication and characterization of an EUV transmission phase grating that overcomes these limitations, allowing optimal accuracy to be obtained.

The PS/PDI is briefly described here; more complete descriptions have been published previously (Medecki *et al.*, 1996; Goldberg, 1997). The PS/PDI is a variation of the conventional point diffraction interferometer (Linnik, 1933; Smartt & Steel, 1975) in which a transmission grating beamsplitter has been added to greatly improve the optical throughput of the system and to add phase-shifting capability. In the PS/PDI (Fig. 1), the optical system under test is coherently illuminated by a spherical wave generated by diffraction from a pinhole placed in the object plane. A grating placed either before or after the test optic is used as a beamsplitter, creating the requisite test and reference beams. A mask (the 'PS/PDI mask' in Fig. 1) is placed in the image plane of the test optic to block unwanted diffracted orders generated by the grating. The mask also serves to spatially filter the reference beam using a second pinhole (the 'reference pinhole'), thereby removing the aberrations imparted by the optical system. The test beam, which also contains the aberrations imparted by the optical system, is largely undisturbed by the image-plane mask: it passes through a window in the PS/PDI mask that is large relative to the diameter of the optical system point-spread function (PSF). The test and reference beams propagate to the mixing plane where they overlap to create an interference pattern recorded on a CCD detector. The recorded interferogram yields information on the deviation of the test beam from the nominally spherical reference beam.

2. Motivation

As with all reference-wave interferometers, the ultimate accuracy of the PS/PDI is limited by the quality of the reference wave. In the case of the PS/PDI, the reference wave is generated by pinhole diffraction and tests have shown the accuracy to improve significantly as the pinhole size is decreased. Ideally, the pinhole should be made substantially smaller than the diffraction-limited resolution of the optic under test. Under these conditions, null tests have demonstrated a reference wavefront accuracy of better than $\lambda_{EUV}/350$ (0.04 nm at λ_{EUV} = 13.4 nm) (Naulleau *et al.*, 1999).

In practice, however, it is difficult to achieve this accuracy due to potential errors imparted by the grating. Line-placement errors in the grating are mapped to wavefront errors in the diffracted wavefront. Because the undiffracted beam (the zero order of the grating) is immune to these errors, the PS/PDI was initially implemented using the zero order as the test beam and the first-diffracted order as the reference beam. In this configuration (the first-order-

reference configuration), aberrations imparted by grating line-placement errors are filtered by the reference pinhole. A drawback of this configuration, however, is that it leads to low fringe contrasts when small pinholes are used or large aberrations are present. This problem is a consequence of the amplitude transmission gratings currently used in the EUV PS/PDI. With amplitude gratings, the first-order-reference configuration can at best provide a one-to-one reference-to-test-beam power ratio as defined prior to the filtering loss induced by the image-plane pinhole. When high accuracy is sought and small pinholes are used, this filtering loss becomes significant, leading to a large power mismatch between the two beams. The same is also true when the test optic contains large aberrations leading to a large PSF. Power mismatch between the test and reference beams yields interferograms of low contrast that are susceptible to noise, including photon, detector-quantization and other camera noise terms. Therefore, the power mismatch places practical limits on the minimum pinhole size, and the size of the aberrations that can be measured in the first-order-reference configuration. In practice, the contrast-limited accuracy in the first-order-reference configuration has been found to be of the order of $\lambda_{EUV}/100$ (Naulleau *et al.*, 1999).

Because gratings with line-placement errors significantly smaller than $T/100$ can readily be fabricated (T being the period of the grating), it is actually beneficial to reverse the beams used as the reference and test waves. In this zero-order-reference configuration, arbitrarily high reference-to-test-beam power ratios can be achieved by using binary gratings with duty cycles other than 50%. In principle, the grating duty cycle can be chosen to exactly balance the filtering loss, which depends both on the aberrations in the test optic and on the size of the reference pinhole. As discussed above, however, the drawback of this approach is that grating errors are directly coupled into the measurement. Tests have shown these errors to limit the accuracy of the PS/PDI to approximately $\lambda_{EUV}/330$ when using high-quality gratings fabricated by electron-beam lithography. Although the zero-order-reference configuration is an improvement over the first-order-reference configuration, achieving full reference-wave limited accuracy requires a different approach.

By using phase gratings it is possible to both achieve an arbitrarily high reference-to-test-beam power ratio and to use the diffracted beam as the reference. In this way we can balance for the use of extremely small pinholes and avoid line-placement errors from coupling into the measurement.

3. EUV phase grating design

Owing to system implementation issues, gratings used with the EUV PS/PDI are ideally of the transmission type. Although reflection EUV phase gratings have been previously described (Underwood *et al.*, 1995), to the best of our knowledge the work presented here represents the first demonstration of high-efficiency transmission EUV phase gratings. While it is difficult to find pure phase-shifting materials at EUV wavelengths, there are various candidate materials that have attractive absorption to phase-shifting ratio properties.

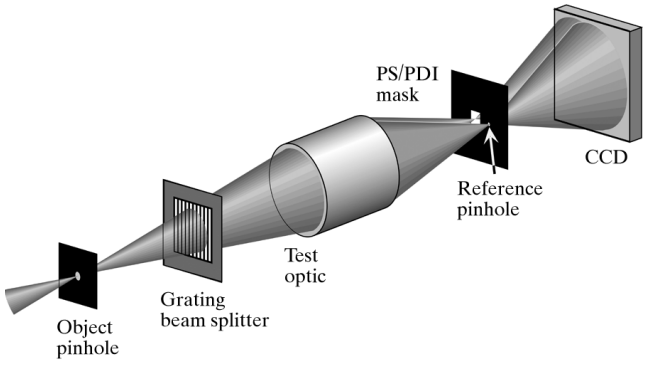

Figure 1
Schematic diagram of the phase-shifting point diffraction interferometer (PS/PDI).

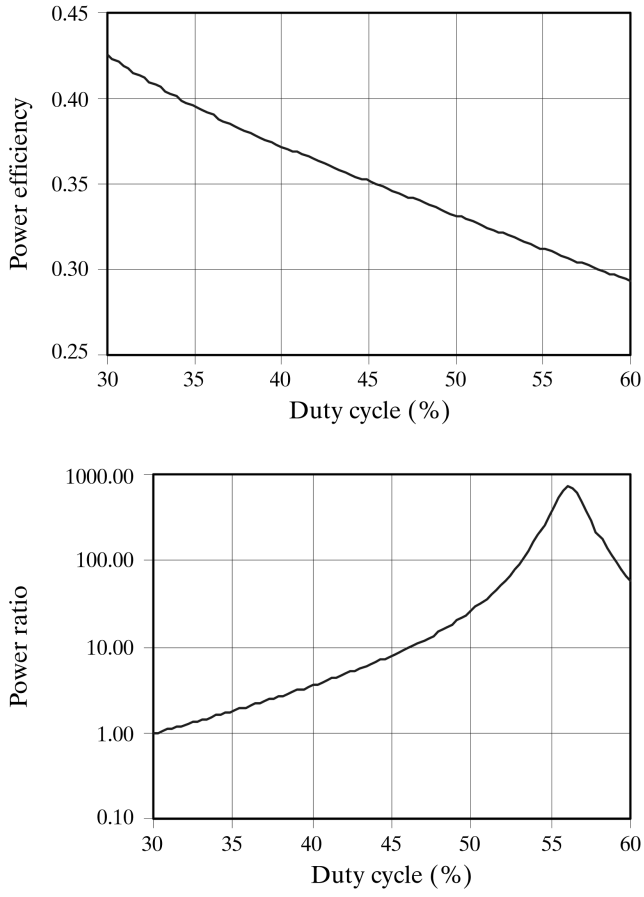

Figure 2
Power efficiency (sum of +1 and 0 order power relative to input power) and +1 to 0 order power ratio for a molybdenum π-phase square-wave grating as a function of duty cycle.

One of the best available materials for phase shifting at EUV wavelengths is molybdenum (Mo). At a wavelength of 13.4 nm, Mo has a *Delta* (the decrement from unity of the real part of the complex index of refraction) of 7.73×10^{-2} and a *Beta* (the imaginary part of the index of refraction) of 6.23×10^{-3} (Henke *et al.*, 1993). From these values we find the 1/e attenuation length of Mo to be 171 nm and the 2π-phase-shift length to be 173 nm. For a π-phase-shift thickness the transmission intensity at a wavelength of 13.4 nm is approximately 60%.

Calculating the diffraction efficiency for a Mo π-phase 50% duty-cycle binary grating, we find the first-to-zero-order power ratio to be 26. This is a significant improvement over the value of 0.4 obtained for a similar amplitude grating. Furthermore, the total efficiency, as measured as the sum of the power in the zero order and one of the first diffracted orders, is almost identical in both cases. This measure is significant because these are the two orders used by the PS/PDI, and thus relate directly to measurement throughput.

In order to compensate for a range of reference pinhole sizes, it is important to be able to tune the power ratio during fabrication. Fig. 2 shows the total power efficiency (sum of +1 and 0 order power relative to input power) and power ratio as a function of duty cycle for a Mo π-phase grating. A duty cycle of 100% represents a solid Mo structure. The power efficiency is seen to monotonically decrease with increasing duty cycle, dropping to a value of ~29% at a duty cycle of 60%. This drop in efficiency with increasing duty cycle is due to the absorption of Mo. The power ratio, on the other hand, shows the interesting behavior of varying by more than two orders of magnitude across the 40% to 60% duty cycle range with the peak occurring at a duty cycle of approximately 56%. From this we see that the power ratio can be readily tuned to a specific experimental situation by choosing the proper grating, thereby balancing the reference beam losses incurred in the PS/PDI.

Another important design and fabrication metric is the actual phase shift imparted by the phase-shifting material (modulation depth). Fig. 2 was based on the ideal zero-absorption modulation depth of π. Fig. 3, on the other hand, shows the power efficiency and power ratio for a 50% duty-cycle phase grating as the modulation depth is varied from 0.8π to 1.2π. The power efficiency is minimum and the power ratio is maximum near π. The exact power ratio peak, however, occurs at approximately 0.99π (86 nm for Mo at $\lambda = 13.4$ nm). This is due to the fact that Mo is not a pure phase-shift material at EUV wavelengths.

Further improvements are possible by using blazed phase gratings; however, these are considerably more difficult to fabricate.

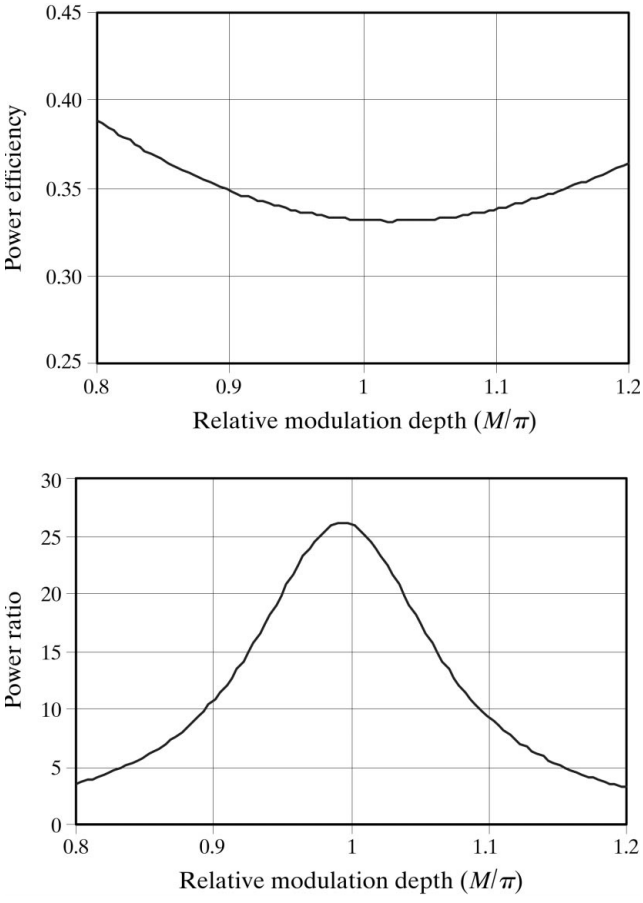

Figure 3
Power efficiency (sum of +1 and 0 order power relative to input power) and +1 to 0 order power ratio for a molybdenum square-wave grating as a function of modulation depth relative to π.

4. Molybdenum grating fabrication

Mo phase gratings have recently been fabricated on silicon nitride (Si_3N_4) membranes patterned into silicon substrates (Fig. 4). A variety of grating pitches were fabricated ranging from 4 μm to 200 μm, all with fabrication goals of π-phase heights and 50% duty cycle. The fabrication process is described as follows. A 1000 Å-thick film of low-stress off-stoichiometric (silicon rich) Si_3N_4 was deposited on both sides of a silicon wafer using low-pressure chemical vapor

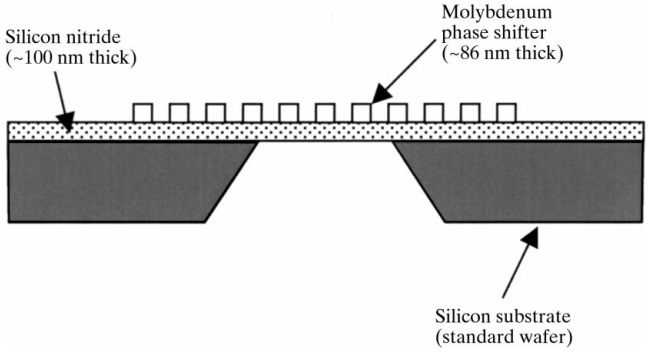

Figure 4
Schematic cross section of the fabricated Mo grating.

deposition (LPCVD). The nitride on the back was patterned and etched, exposing the silicon substrate. Mo was then deposited on the front-surface silicon nitride by magnetron sputtering. To reduce the stress in the Mo film, the sputtering conditions were optimized, *i.e.* plasma power and sputtering pressure were set to approximately 100 W and 90 mtorr, respectively. Under these conditions the deposition rate was $\sim$190 Å min^{-1}. At lower pressures, around 50 mtorr, the Mo deposition rate was lower and excessive stress in the Mo film caused the Si_3N_4 membranes to break during the final stage of fabrication.

After deposition of the Mo, photolithography and etch processes were used to delineate the grating lines. After etching, the thickness of the remaining Mo was measured with a stylus profiler to vary between 750 Å and 1000 Å. The target thickness for a π-phase shift was 865 Å. Owing to process errors in the photolithography step and etch skew, the line widths of the Mo features were about 2 μm smaller than expected at the top of the feature. This caused the final effective duty cycle of the gratings to range from approximately 30% for the 6 μm pitch to the desired 50% for pitches of 100 μm and larger. The 4 μm pitch gratings failed completely. In order to make a transmission structure, the silicon wafer was etched in KOH solution from the back, stopping on the front-surface Si_3N_4. To protect the Mo patterns during the silicon etch, oxide was deposited on top of the Mo patterns using plasma-enhanced chemical vapor deposition (PECVD).

5. Grating characterization

The Mo gratings were characterized at the calibration and standards bend-magnet beamline 6.3.2 (Underwood *et al.*, 1996) at the Advanced Light Source located at Lawrence Berkeley National Laboratory. The measurements were performed at a wavelength of 13.4 nm and a spectral resolution, $\lambda/\Delta\lambda$, of approximately 1400. The qualitative performance of the gratings was visualized by imaging the exit slit of the beamline monochromator through the phase grating onto a fluorescent screen. This screen was in turn imaged by a CCD camera. Fig. 5 shows the results for grating pitches of 12, 8 and 6 μm. For pitches of 12 and 8 μm, the gratings display the desired behavior of zero-order suppression relative to the ±1 diffracted orders. The effect breaks down in the 6 μm pitch case, however, due to fabrication problems associated with the fine 3 μm features. As described above, etch skew was observed to have significantly affected these structures. The configuration of the measurement system precluded observing larger pitch gratings due to insufficient order separation in the observation plane.

More quantitative data were collected by replacing the fluorescent screen with a large area detector and scanning it across the diffraction pattern in the direction of the grating diffraction. This method records the integral of the diffraction pattern, which can be numerically differentiated to reconstruct a quantitative measure of the diffraction efficiency (power ratio). Fig. 6 shows plots of the reconstructed transmitted intensity as a function of output angle. The total throughput of the gratings was measured to be (40.2 ± 0.2)% for the 12 μm- and 8 μm-pitch gratings, and (41.8 ± 0.2)% for the 6 μm-pitch grating. Depending on the exact material characteristics of the Si_3N_4 membrane

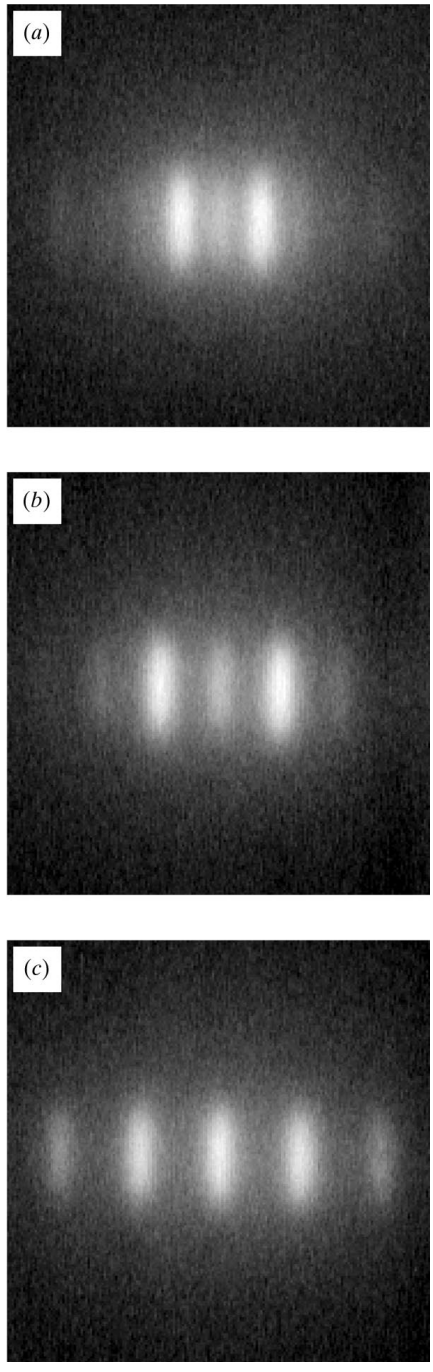

Figure 5
Grating far-field diffraction patterns. The exit slit of the beamline monochromator was imaged through the phase grating onto a fluorescent screen, which was in turn imaged by a CCD camera. Results for grating pitches of (*a*) 12 μm, (*b*) 8 μm and (*c*) 6 μm are shown.

(which we did not independently characterize), the theoretical throughput lies in the 40% to 45% range.

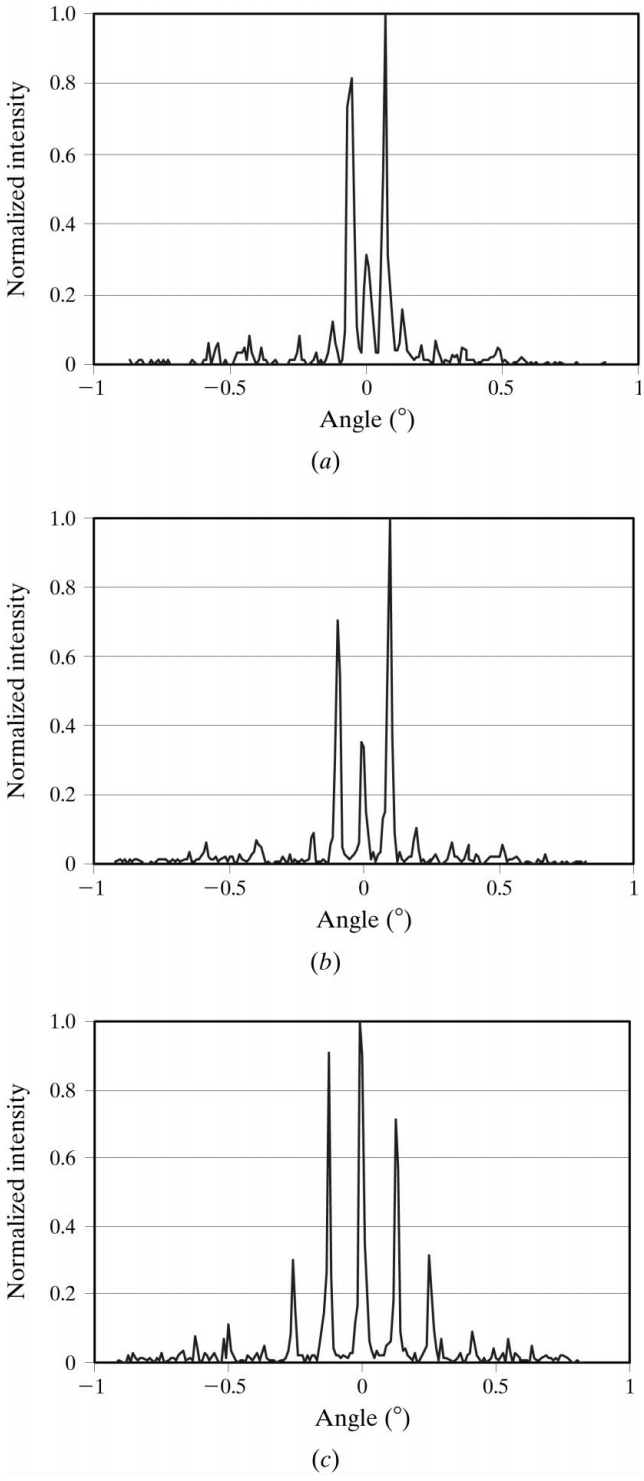

Figure 6
Reconstructed transmitted intensity as a function of output angle. These data were collected by replacing the fluorescent screen with a large area detector and scanning it across the diffraction pattern. This method records the integral of the diffraction pattern, which can be numerically differentiated to reconstruct a quantitative measure of the diffraction efficiency. Results for grating pitches of (*a*) 12 μm, (*b*) 8 μm and (*c*) 6 μm are shown.

The power ratio (first-diffracted-order power divided by zero-order power) is determined from the integrated energy in each diffraction peak. This yields power ratios of 0.69 ± 0.01, 1.9 ± 0.1 and 2.4 ± 0.1 for the 6 μm-, 8 μm- and 12 μm-pitch gratings, respectively. The asymmetry seen in the diffracted orders (Fig. 6) is most likely due to asymmetric etch skew and has been taken into account in the quoted uncertainties of the measured power ratios. From the measured power ratios we predict the effective duty cycles of the gratings to be approximately 27%, 36% and 37% for the 6 μm-, 8 μm- and 12 μm-pitch gratings, respectively.

The duty cycles predicted for the 8 μm- and 12 μm-pitch gratings are within 10% of the values determined from scanning electron microscope measurements, whereas the 6 μm-pitch case shows a difference of approximately 20%. This discrepancy is most likely due to the more complicated geometry induced by the etch skew. These measurements indicate the actual grating heights to be within 10% of the desired π-phase height of 86.5 nm, in agreement with the stylus profiler results described above.

The duty cycles determined above are also consistent with the measured relative output power efficiencies (sum of +1 and 0 order power relative to total output power). For the 8 μm- and 12 μm-pitch gratings we obtain power efficiencies of $(45 \pm 2)\%$ and $(46 \pm 2)\%$, whereas the ideal efficiencies using the duty cycles predicted from the measured power ratios are 46% and 45%, respectively. The ideal values are readily obtained from Fig. 2 taking into consideration the 60% transmission of a π-phase-length thickness of Mo. For the 6 μm-pitch case, however, the agreement was not as good; the measured efficiency was $(54 \pm 2)\%$ and the predicted efficiency was 50%. Again, this is believed to be a result of the etch-skew problem.

6. Conclusions

Transmission phase gratings operational at EUV wavelengths with high throughput and relatively high diffraction efficiency have been fabricated and characterized. These gratings hold great promise for improving the throughput and accuracy of diffraction-based EUV interferometers. Such interferometers include the PS/PDI described here as well as EUV shearing interferometers (Bjorkholm *et al.*, 1995; Ray-Chaudhuri *et al.*, 1995). Obtaining first-to-zero-order power ratios of 100 and greater will require improved process control. Improvement of the Mo deposition and etch process is currently being pursued, including the use of a dry etch procedure.

The authors are greatly indebted to Kenneth Goldberg for many enlightening discussions. This research was supported by the Extreme Ultraviolet Limited Liability Company, the Semiconductor Research Corporation, DARPA Advanced Lithography Program, and the DOE Office of Basic Energy Science.

References

Bjorkholm, J. E., MacDowell, A. A., Wood, O. R. II, Tan, Z., LaFontaine, B. & Tennant, D. M. (1995). *J. Vac. Sci. Technol. B*, **13**, 2919–2922.

Goldberg, K. A. (1997). PhD dissertation, University of California, Berkeley, USA.

Henke, B. L., Gullikson, E. M. & Davis, J. C. (1993). *Atom. Data Nucl. Data Tables*, **54**, 181–342.

Linnik, W. (1933). *Proc. Acad. Sci. USSR*, **1**, 210–212.

Medecki, H., Tejnil, E., Goldberg, K. A. & Bokor, J. (1996). *Opt. Lett.* **21**, 1526–1528.

Naulleau, P., Goldberg, K. A., Lee, S., Chang, C., Attwood, D. & Bokor, J. (1999). *Appl. Opt.* **38**, 7252–7263.

Ray-Chaudhuri, A. K., Ng, W., Cerrina, F., Tan, Z., Bjorkholm, J., Tennant, D. & Spector, S. J. (1995). *J. Vac. Sci. Technol. B*, **13**, 3089–3093.

Smartt, R. N. & Steel, W. H. (1975). *Jpn. J. Appl. Phys. Suppl.* **14**(1), 351–356.

Tejnil, E., Goldberg, K. A., Lee, S. H., Medecki, H., Batson, P. J., Denham, P. E., MacDowell, A. A., Bokor, J. & Attwood, D. (1997). *J. Vac. Sci. Technol. B*, **15**, 2455–2461.

Underwood, J. H., Gullikson, E. M., Koike, M., Batson, P. J., Denham, P. E., Franck, K. D., Tackaberry, R. E. & Steele, W. F. (1996). *Rev. Sci. Instrum.* **9**, 1–5.

Underwood, J. H., Malek, C. K., Gullikson, E. M. & Krumrey, M. (1995). *Rev. Sci. Instrum.* **66**, 2147–2150.